EUMETSAT AC SAF
ATMOSPHERIC COMPOSITION MONITORING

ALGORITHM THEORETICAL BASIS DOCUMENT

IASI NH_3

Prepared by	Lieven Clarisse Martin Van Damme Bruno Franco Daniel Hurtmans Rosa Astoreca Pierre-François Coheur Cathy Clerbaux	October 25th, 2021

TABLE OF CONTENTS

1. INTRODUCTION

1.1 Objective

This document describes the NH_3 retrieval algorithm (level 2) for IASI onboard Metop-A, B, and C, developed at ULB and for which an implementation at EUMETSAT has been agreed in the frame of the AC SAF CDOP-3 project. The retrieval algorithm is part of a chain of retrieval algorithms called the ANNI (Artificial Neural Network for Infrared Atmospheric Sounding Interferometer, IASI) retrieval framework, for the retrieval of short and medium long-lived trace gases, see Franco et al. (2018). The historical development, theoretical basis and background has been documented in a series of papers: Whitburn et al. (2016), Van Damme et al. (2017), Franco et al. (2018) and Van Damme et al. (2021). Most of the text and some figures below are taken verbatim from these publications without referencing these explicitly each time. Some material is also taken from Clarisse et al. (2019).

1.2 IASI instrument

IASI is an infrared Fourier transform spectrometer developed jointly by CNES (the French space agency) with support of the scientific community (for a review see Hilton et al. (2011)), and by EUMETSAT. IASI is mounted on-board the European polar-orbiting Metop satellite with the primary objective to improve numerical weather predictions, by measuring tropospheric temperature and humidity with high horizontal resolution and sampling, with 1 km vertical resolution, and with respectively 1 K and 10% accuracy (Camy-Peyret and Eyre, 1998). As a second priority, IASI contributes to atmospheric composition measurements for climate and chemistry applications (Clerbaux et al., 2009). To reach these two objectives, IASI measures the infrared radiation of the Earth's surface and of the atmosphere between 645 and 2760 cm^{-1} at nadir and along a 2200 km swath perpendicular to the satellite track. A total of 120 views are collected over the swath, divided as 30 arrays of 4 individual Field-of-views (FOVs) varying in size from $6 \times 6 \times \pi$ km^2 at nadir (circular 12 km diameter pixel) to $10 \times 20 \times \pi$ km^2 at the larger viewing angle (ellipse-shaped FOV at the end of the swath). IASI offers in this standard observing mode global coverage twice daily, with overpass times at around 9:30 and 21:30 mean local solar time. The very good spatial and temporal sampling of IASI is complemented by fairly high spectral and radiometric performances: the calibrated level 1C radiances are at 0.5 cm^{-1} apodized spectral resolution (the instrument achieves a 2 cm optical path difference), with an apodized noise that ranges below 2500 cm^{-1} between 0.1 and 0.2 K of a reference blackbody at 280 K (Hilton et al., 2011).

1.3 Retrieval overview

A schematic overview of the ANNI retrieval is presented in Figure 1. The actual calculation of the columns (red boxes in Figure 1) relies on two computational steps:

1. The calculation for each IASI observation of a hyperspectral range index (HRI). This quantity is a very sensitive, broadband spectral index that quantifies the signal strength of a target absorber in a radiance spectrum.

2. The conversion of the HRI into a total column abundance via an artificial feedforward neural network (NN).

In addition to the HRI, the NN relies on a series of auxiliary parameters related to the state of the atmosphere and of the surface. Perturbations to the input data of the NN allows quantification of the uncertainties associated with single-pixel retrieved columns. Appropriate filtering of the data (before and after the retrieval) removes cloudy scenes and observations with limited or no sensitivity to the target trace gas. Finally, in general (for most species in the ANNI retrieval framework), a calibration offset is added to the retrieved columns to account for the constant, climatological background column of the target gas in the atmosphere (green box in Figure 1). However, this last step is not done for NH_3, as background concentrations are extremely low and below the detection limit of IASI.

While the retrieval itself is simple and fast, the initial setup (blue and red boxes in Figure 1) of the HRI and NN is nontrivial. In particular, both rely on weight constants that must be determined with care beforehand from a data set of real (for the HRI) and synthetic (for the NN) IASI spectra. The setup of the HRI and NN and the training of these weight constants is detailed in sections 2.1 and 2.2. The actual retrieval and examples are presented in section 2.3.

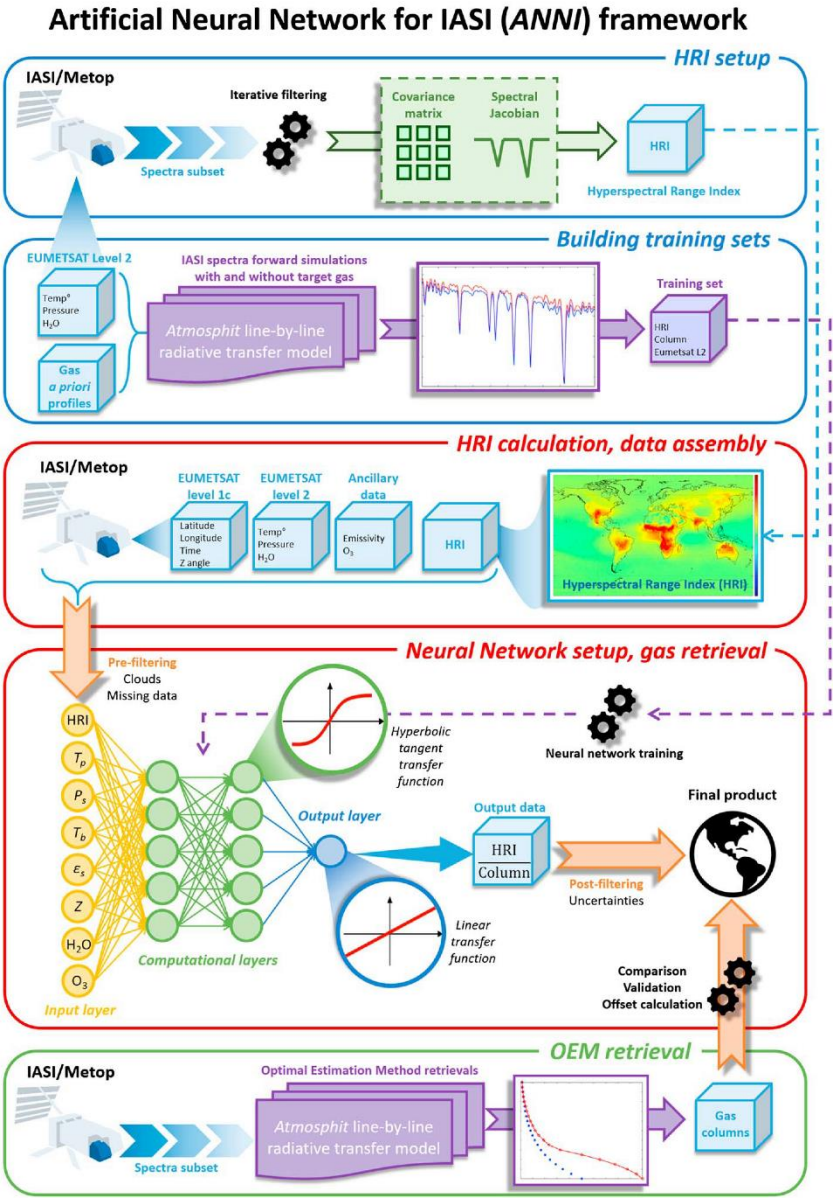

Figure 1. Conceptual flowchart of the ANNI retrieval method of trace gases.

2. ALGORTIHM DESCRIPTION

2.1 HRI

2.1.1 Definition

Proposed by Walker et al. (2011), the HRI is a dimensionless index that quantifies the strength of the spectral signature of a target gas in an observed spectrum y:

$$\mathrm{HRI} = \frac{K^T S_y^{-1}(y-\bar{y})}{\sqrt{K^T S_y^{-1} K}} \frac{1}{N} \quad (1)$$

where K is a spectral Jacobian, S_y a covariance matrix, and $\bar{y}$ the mean spectrum generated from a representative data set of background spectra associated with a climatological column of the target gas, and N an extra normalization factor (see further). The HRI is conveniently normalized to have a mean of zero and a standard deviation of one when calculated on the data set of background spectra. The HRI is particularly suitable for the detection of highly variable infrared absorbers, like NH_3, which are not observed in every spectrum. In this case, the climatological column amount is close to zero and the background spectra are those without observable signature of NH_3. The HRI can encompass spectral ranges of up to several hundred cm^{-1} to exploit all the channels in which the target species is absorbing. This results in a substantial gain of sensitivity over other detection methods and makes it highly suitable for the detection of broadband absorption features, as demonstrated with the detection of a series of aerosol types in Clarisse et al. (2013).

2.1.2 Spectral range and Jacobian

Larger spectral ranges lead in principle to a more sensitive HRI. However, this is true only in the linear regime in which the covariance matrix describes a normal distribution. In practice, it can be advantageous to exclude spectral ranges where nonlinearity prevails. For instance, the spectral range 1,100–1,200 cm^{-1} can exhibit pronounced spectral surface emissivity features over deserts. In addition, it might be useful to avoid a spectral interval in which another species with a similar spectral signature is absorbing. For NH_3 the range was set to 812–1,126 cm^{-1} that exploits the strongest lines from its ν_2 vibrational band. The range was not chosen larger to minimize interferences with surface emissivity features. The Jacobian K is the derivative of the radiance spectrum with respect to the column abundance of the target species, and this was generated by the line-by-line radiative transfer model Atmosphit (Coheur et al., 2005) for a standard atmosphere.

2.1.3 Characterization of mean and covariance

For each target species, the HRI calculation also depends on a generalized covariance matrix S_y and an associated background spectrum $\bar{y}$. The covariance matrix determines the weight of each spectral channel, and ideally expresses the variability and covariance of all interfering species, but explicitly not that of the target species (Walker et al., 2011). Such a matrix can be obtained from a representative set of IASI spectra with a constant, climatological column amount of the target species. For short-lived trace gas absorbers like NH_3, the pair (S_y, $\bar{y}$) can straightforwardly be constructed from spectra with no observable signature of the gas (the

associated climatological column is then close to zero). To select such spectra, an iterative approach can be followed (Clarisse et al., 2013). The approach goes like this. First, a representative set of IASI spectra is build, consisting of all the spectra from the fifteenth of each month of 2013 but sampled to yield a spatially uniform distribution (to avoid over-representing polar regions). This entire set is then used for the generation of a first (S_y, $\bar{y}$) pair. This allowed the production of a first set of HRI, which in turn was used to remove the spectra with detectable signatures of the trace gas (typically with an HRI above 3 or 4; see below). The reduced set of spectra allows the calculation of a better (S_y, $\bar{y}$) pair. Repeating this process several times (typically at least 10 times) leads to convergence of the set of spectra, of the corresponding (S_y, $\bar{y}$), and of the HRI.

An even more sensitive HRI could be constructed by considering only the spectra with an HRI below one. Using such a low threshold removes much more spectra; including those with spectral signatures barely above the instrumental noise and even spectra without detectable gas quantities. This is obvious for NH_3, where spectra above remote oceans frequently exhibit HRIs below one. Nevertheless, removing such spectra leads to a more sensitive HRI and does not generate anomalies (e.g., false detections). There is, however, a side effect, in that the initial normalization of the HRI is not preserved in the iterative process. This is the reason why an additional normalization factor (N) is needed in equation (1). Note that this factor N needs to be recalculated at each iteration. The normalization factor N was calculated as the standard deviation of the HRI over a remote ocean area, where no NH_3 is expected.

In total 24 iterations were carried out for the construction of the covariance matrix. In addition to all observations with an HRI below one, also observations over selected desert regions were included at each iteration, as no NH_3 is expected for those, and to make the HRI more robust for the emissivity features found over deserts.

2.1.4 Detrending and anomaly correction

Analysing the initial time series of the mean HRI over remote oceans, we noticed (i) offsets that coincided with changes to the IASI instrument, (ii) a slowly decreasing trend and (iii) a residual dependence on H_2O. In the rest of the section we outline the first order corrections that were introduced to account for all of these. Referring to Figure 2, the following corrections were introduced:

(b) The declining trend over remote areas that was identified in the HRI of NH_3 is apparent in the top panel of Figure 2. As the trend is linear, and as there are a couple of weak CO_2 absorption bands in the 812–1126 cm^{-1} spectral range, this trend is most likely due to the ever increasing concentrations of CO_2 . To correct this bias, we analyzed monthly averaged HRI from IASI spectra measured over a remote location in the Pacific Ocean (17°N–22°N; 153°W–158°W) versus time. The linear regression ($y = -8.69 \times 10^{-5} x + 63.75$, $r = -0.84$, with x and y being the time (in months) and the HRI (no unit), respectively) models the relationship well and was therefore used to apply a first-order correction to the calculated HRI.

(c) A change in the IASI Level 1C occurred on 18 May 2010 and corresponds to an improvement of the spectral calibration. An empirical correction was introduced as a function of latitude and day of the year. The precise offsets were computed as the difference between the median HRI calculated before and after the 18 May 2010, the median being calculated in 1° latitude bins from all the HRI with an absolute longitude above 160° and an absolute value below 5. This difference was calculated for each day of the year and applied to the HRI calculated before the 18 May 2010 (Figure 2, panel (c)).

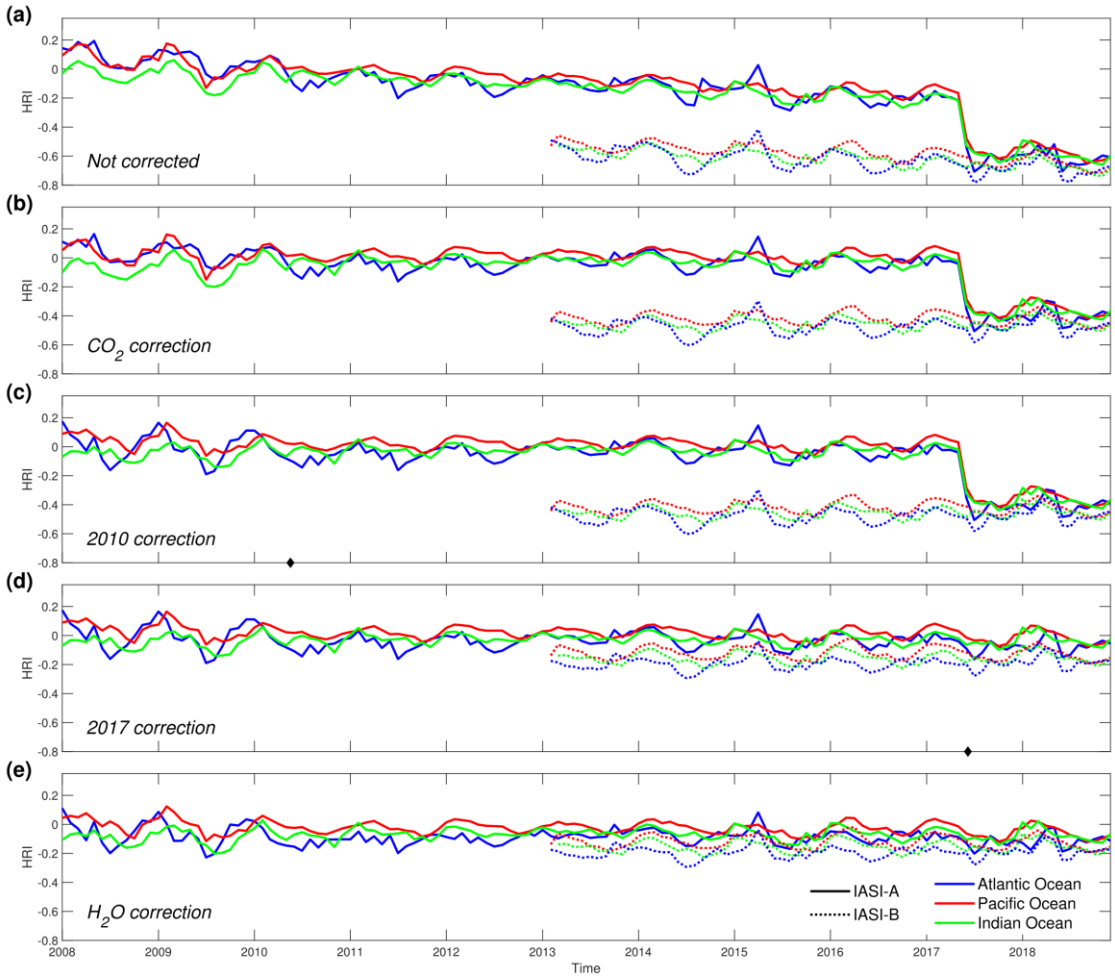

Figure 2 IASI/Metop-A (solid lines) and IASI/Metop-B (dashed lines) NH_3 Hyperspectral Range Index (HRI, no unit) monthly time series over three remote locations: North Atlantic Ocean (20°N–40°N; 30°W–60°W), Pacific Ocean (0°S–30°S; 125°W–175°W) and Indian Ocean 5°S–25°S; 55°E–95°E). From top to bottom: (a) not corrected time series and successive implementation of corrections (b)–(e).

(d) On 7 June 2017, a minor change in the configuration parameters for the apodization function of IASI/Metop-A instrument had a clear impact on the calculated HRI (Figure 2, panels (a)–(c)). This recalibration made IASI/Metop-A more in line with IASI/Metop-B instrument. As the HRI is based on a covariance matrix from spectra of the year 2013, the HRI calculated after the recalibration for IASI/Metop-A have to be adjusted, as well as the entire time series of IASI/Metop-B. Comparison of the HRI values on 6 June with the ones from 8 June 2017, revealed a temperature dependence in the offset. A satisfactory correction was obtained using a linear regression ($y = -3.5 \times 10^{-3}\ x - 0.69$, $r = 0.89$, with x being the temperature of the baseline (in K) and y the median of the HRI difference between the 6 and the 8 June 2017 (no unit); see Figure 2, panel (d)).

(e) Finally, a H_2O correction was implemented, as a dependence of the HRI to H_2O was found over remote oceans. This does not change the behaviour of the HRI over time, but helps to debias it. A H_2O-dependent bias was determined from a region assumed NH_3-free by calculating the median over sea for 30 days in 2015 over bins of 0.1×10^{23} molec cm^{-2} of H_2O total column. These median values are then used to correct the HRIs before using them as an input in the neural network (i.e. after the correction, the mean HRI over remote oceans is closer

to zero). Panel (e) of Figure 2 presents the corrected monthly time series of HRI over three remote locations. It shows that the corrections allow us to obtain a coherent time series over the IASI operating period, centred around zero and as expected without noticeable jumps or trends.

2.2 The neural network

The spectral signature (the HRI) of a target gas is a complex function of the species abundance and of all the other parameters entering into the radiative transfer, such as the state of the atmosphere (thermodynamic parameters) and surface, interfering species, and the viewing angle. The main idea of the current retrieval approach is to use a NN to approximate the complex inverse function that maps the HRI and the auxiliary parameters to a column abundance. A NN consists of interconnected nodes (small mathematical functions) organized in layers, as illustrated in Figure 1 (lower red box). The weights of the nodes are trained to best fit the complex analytical relationships that bind any set of input variables feeding the network, to the corresponding output variable. NNs learn from the presentation of examples, and so training sets are required consisting of matching input (auxiliary parameters, column abundance) and output data (IASI spectrum and associated HRI). The construction of these training sets are detailed in the next section. We also describe the setup of the network, the training itself and the performance on the training set.

2.2.1 Training Set Assembly

The performance of a NN depends largely on the quality of the training set, which should be as comprehensive and representative as possible. This means that in our case, the set should cover a large range not only of the column abundances of the target trace gas (and associated HRI) but also of the auxiliary parameters on the state of the atmosphere and surface. Each IASI observation (L1C radiance spectra) is distributed operationally with corresponding Level 2 data consisting of a temperature, pressure, H_2O profile, and surface temperature (August et al., 2012). These were used here as input for the auxiliary parameters of the training data set. We selected approximately 500,000 IASI L2 data over the year 2013, regularly sampled in space and time to ensure a comprehensive and representative data set.

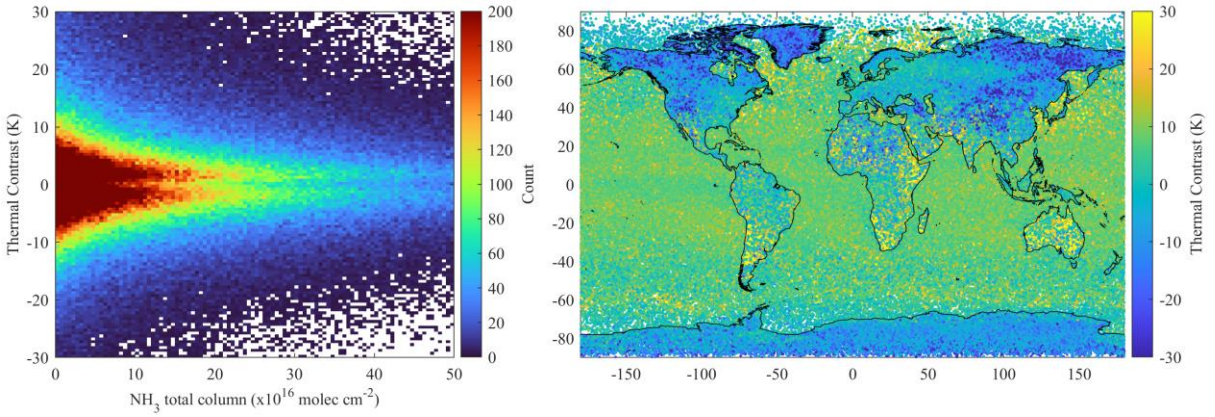

Figure 3 Summary statistics on the training set: distribution of thermal contrast vs NH_3 total columns (left), and spatial distribution vs thermal contrast (right).

As the surface temperature and emissivity vary more over land than over oceans, 66 % of the data were chosen to be associated with land observations. Additional data were added for the

higher and lower thermal contrasts TCs (defined as the temperature difference between the surface and the air layer located just above) to ensure that extreme TCs are sufficiently represented within the training data set. Finally, a random column of the target trace gas was associated with each sample in the data set. These random columns were generated by randomly scaling a vertical profile of the gas (see below) from 1×10^{14} molec/cm^2 up to 5×10^{17} molec/cm^2. Figure 3 illustrates the spatial distribution of the resulting data set as well as the sampling as a function of thermal contrast and total column. IASI spectra were simulated for each sample in this data set using Atmosphit. Due to small remaining forward model errors, it was found that HRI values produced by Atmosphit can be biased. For this reason, a spectrum was simulated for each sample with and without the target trace gas. The HRI of the simulation without the target gas was then used to offset the HRI of the other simulation, in such a way that an HRI value of zero always corresponds to the absence of the trace gas. Note that since Atmosphit does not simulate the clouds, the resulting training data set is cloud-free.

As discussed in Whitburn et al. (2016), the choice of the vertical profile of the target gas used in the forward simulations is important. For this reason, the vertical profile of NH_3 was parameterized with a Gaussian function as

$$\mathrm{NH_3(vmr)} = \mathrm{ScalFact} \cdot e^{-\left(\frac{(z-z_0)^2}{2\sigma^2}\right)} \qquad (2)$$

Two different training sets have been built (see Figure 4): (a) One representative for observations close to emission sources (thus with the peak concentration at the surface), where z_0 was fixed to 0 km and where sigma (σ) was assigned a random number between 100 m and 6 km. (b) One representative for transported NH_3, with a peak concentration above the surface. Here z_0 was assigned a random number between 0 and 20 km.

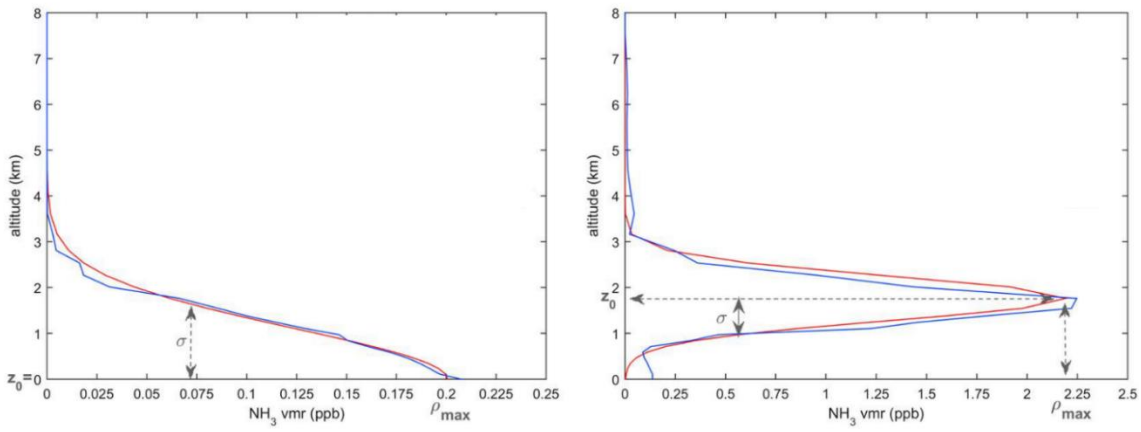

Figure 4 Example of GEOS-Chem model (blue) and fitted (red) profiles (left) above a source area and (right).

2.2.2 Network Setup, Training, and Evaluation

In theory, the input parameters could consist of all the variables used for the forward simulation of the spectra. However, this would result in a very large and difficult data set to train NNs. Instead, it is advantageous to keep the size of the NN as small as possible by only taking into account the parameters that affect most the output variable. A satisfactory network performance was achieved by training with the following input parameters:

- HRI
- temperature profile (T_{prof}) at 0, 0.5, 1, 1.5, 2, 2.5, 3, 5, 7, 10, 13, 16, 19, 25 and 30 km
- skin temperature (T_{skin})

- surface pressure (P_{surf})
- emissivity (ε_{surf}): average over selected channels in the atmospheric windows
- H_2O partial column profile (H_2O_{prof}) between 0-1, 1-2, 2-3, 3-5, 5-7, 7-10 and 10-30 km
- satellite viewing angle (Z)
- peak NH_3 altitude (z_0)
- Spread of the NH_3 profile (σ)

The HRI-to-column ratio was adopted as output of the NN instead of the gas column itself. The rationale behind this is explained in detail in Van Damme et al. (2017) and Whitburn et al. (2016). In brief, using the ratio allows (1) for a better training of the NN owing to its smaller dynamic scale and (2) to translate the instrumental noise—which is part of the HRI—in a linear way to the retrieved column. In particular, this guarantees that the retrieval on noisy HRI does not lead to a biased product. However, the downside is that slightly negative columns can be retrieved because of the noise on the HRI.

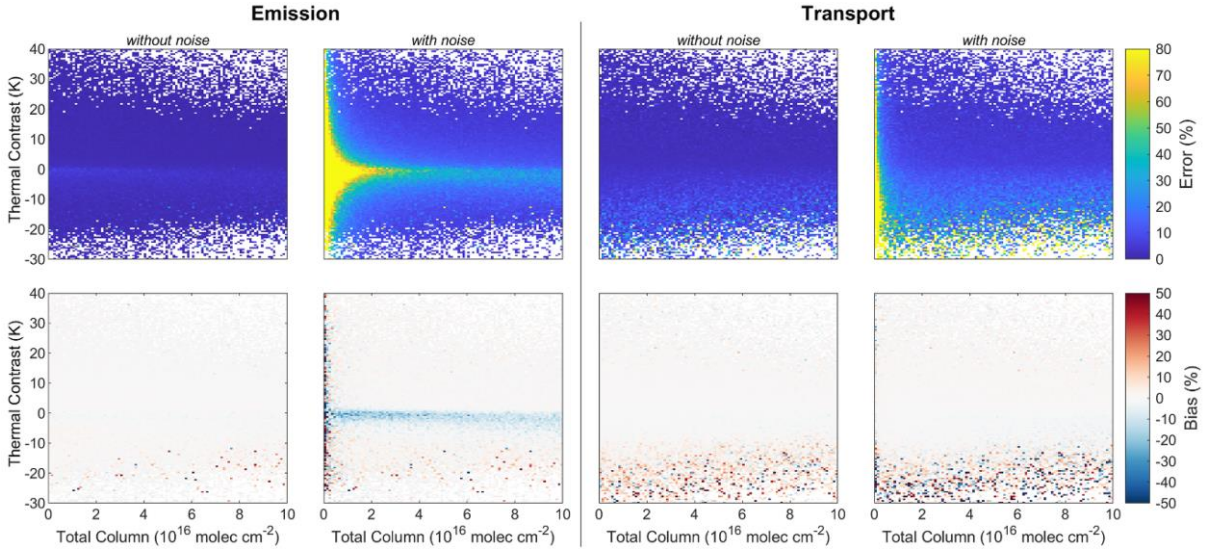

Figure 5 Performance evaluation (top: error, bottom: bias, both in %) of the emission network (left four panels) and transport network (right four panels), with and without adding noise. The median value is shown in each grid box, which removes the effect of outliers and allows us to better assess the real performance of the network.

Based on the training performances, a NN that consists of two computational layers was setup with each 12 nodes. A multilayer NN is usually better at tackling nonlinearities than a many-node, single-layer network. We have evaluated and improved the setup of the different NNs using 2-D error plots. These summarize the performance of the NN on the training set in terms of relative error and biases as a function of gas total column and thermal contrast. The performance plots are presented in Figure 5. Note that normally distributed noise was added to all the input data to evaluate the performances as realistically as possible (right panels). The final NNs are seen to be practically unbiased for positive TC. For the non-background gas abundance, the relative errors range from 10% to 50%, with the highest errors found for the low gas columns. The relative errors increase for lower background columns (top panels in Figure 5) where the columns approach the IASI detection threshold. However, since the biases remain low (bottom panels), most of these errors can be averaged out by considering multiple observations (thus by averaging the retrieved columns in time or space). In addition, as can be expected, the NNs do not perform well for observational scenes with low negative TC.

2.3 Retrieval, Uncertainty and Data Post-filtering

2.3.1 Retrieval

The actual retrieval consists first of collecting the required input data, that is, the HRI of the observed spectrum and the matching auxiliary data. Most of the auxiliary data is directly taken from the IASI L2 (except the viewing angle, which is part of the IASI L1). As the sources of NH_3 are mostly continental, the columns over land that are included in the final ANNI product are those retrieved with the NN developed specifically with the emission profile, assuming z_0=0 and σ equal to the ERA5-derived planetary boundary height monthly day/night climatology (but with the minimum capped at 100 meter, see Figure 6). The latter was built based on over 10 years of ERA5 data (from October 2007 to December 2018). Conversely, the retrievals performed with the transport-NN are used for the measurements over the oceans and we assume z_0 = 1.4 km and σ = 0.905 km (see Whitburn et al., 2016 for a justification). The NN is then fed with these data as illustrated in Figure 1. Finally, the inverse of the HRI-to-column ratio obtained as output of the network is multiplied by the associated HRI, yielding the total column of the target species. Before the different networks are applied to the real IASI measurements, all satellite observations with invalid L1, L2 or with a cloud fraction above 25% inside the IASI field of view are filtered out.

Parameter	Uncertainty
T_{prof}	1 K
H_2O_{prof}	10%
T_{skin}	1 K
Z	0
P_{surf}	500 Pa
ε_{surf}	0.01
z_0	0
σ	100 m
HRI	1

Table 1. Assumed uncertainties on the input parameters.

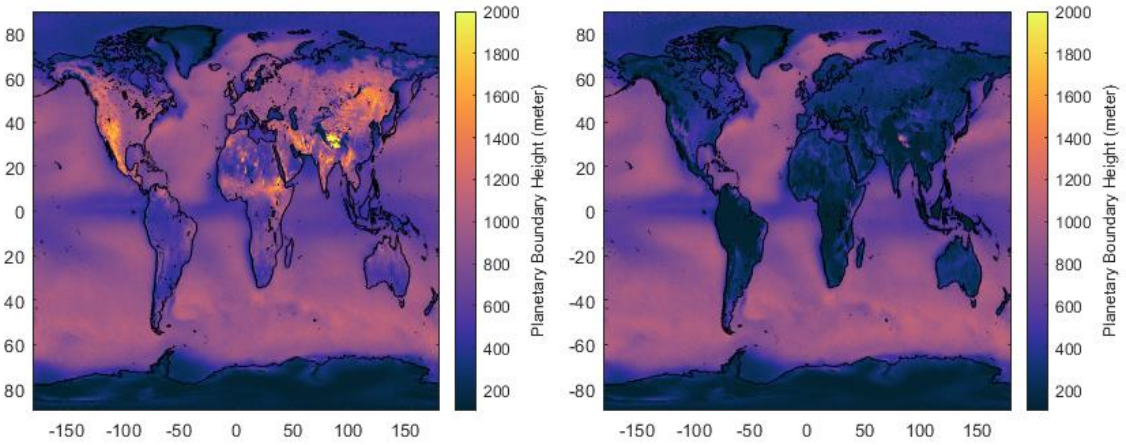

Figure 6 Example ERA 5 climatology of the planetary boundary layer for April, morning (left) and evening (right).

2.3.2 Uncertainty

An (absolute) uncertainty is estimated for each retrieved column, by propagating the uncertainties of the different variables feeding the NN (see Table 1):

$$\sigma_{NH3}^2 = \sqrt{\sum_i \left(\frac{\partial NH_3}{\partial \sigma_i^2}\right)^2 \sigma_i^2} \qquad (3)$$

2.3.3 Quality flag

As the retrieval does not use an a priori, it is poorly constrained in case of low sensitivity. Fortunately, the corresponding measurements can quite readily filtered out. The choice was made to define the retrieved columns into three distinct, mutual exclusives groups:

1. Stringent quality assurance

For these observations, the following conditions are both satisfied:

- $|\ NH_3$ column/HRI $| < 15 \times 10^{15}$ molec/cm^2
- $|\ NH_3\ | > 0$ molec/cm^2 or $|HRI| < 1.5$

2. Weak quality assurance

These are observations, which do pass the stringent quality assurance test, but satisfy the following weaker conditions:

- $|\ NH_3$ column/HRI $| < 30 \times 10^{15}$ molec/cm^2
- $|\ NH_3\ | > 0$ molec/cm^2 or $|HRI| < 1.5$

3. No quality assurance

These are all the remaining observations.

2.3.4 Note on negative columns

The retrieval, by construction can return negative columns (inherited from negative HRIs and the fact that the neural network outputs the HRI-to-column ratios). While these clearly lack a clear physical interpretation, they are an integral part of the product and are not meant to be removed systematically. The use of negative physical quantities in satellite data is not new. They can for instance be found in MODIS AOD data starting from the Collection 5 (Levy et al., 2007). In this paper the authors call such negative values “statistically imperative” for creating an unbiased data set. For IASI observations of NH_3, which are expected to be measurable only in part of the data (i.e., in large areas and or certain periods, the retrieval should ideally average to 0), the necessity of having negative retrievals for an unbiased product becomes even more important. Our retrieval setup deals automatically and in a natural way with the instrumental noise through the output of HRI-to-column ratios. As long as the HRI’s are unbiased, an unbiased product is guaranteed, and the NN does not need to worry about instrumental noise and can assume that the measurements are noise-free.

It is however recommended to remove negative columns from time or space averaged data (an average over a large area, or a seasonal average), as these are not expected to exhibit important negative columns on average.

2.3.5 Example: A single overpass

Example retrievals of the columns and associated uncertainties are shown in Figure 7 for a morning and overpass over Europe respectively. In the morning overpass, thanks to a good thermal contrast, the post filter does not remove many observations (apart from a few large

negative ones). This is in contrast to the evening overpass, where most observations are removed because of lack of sensitivity.

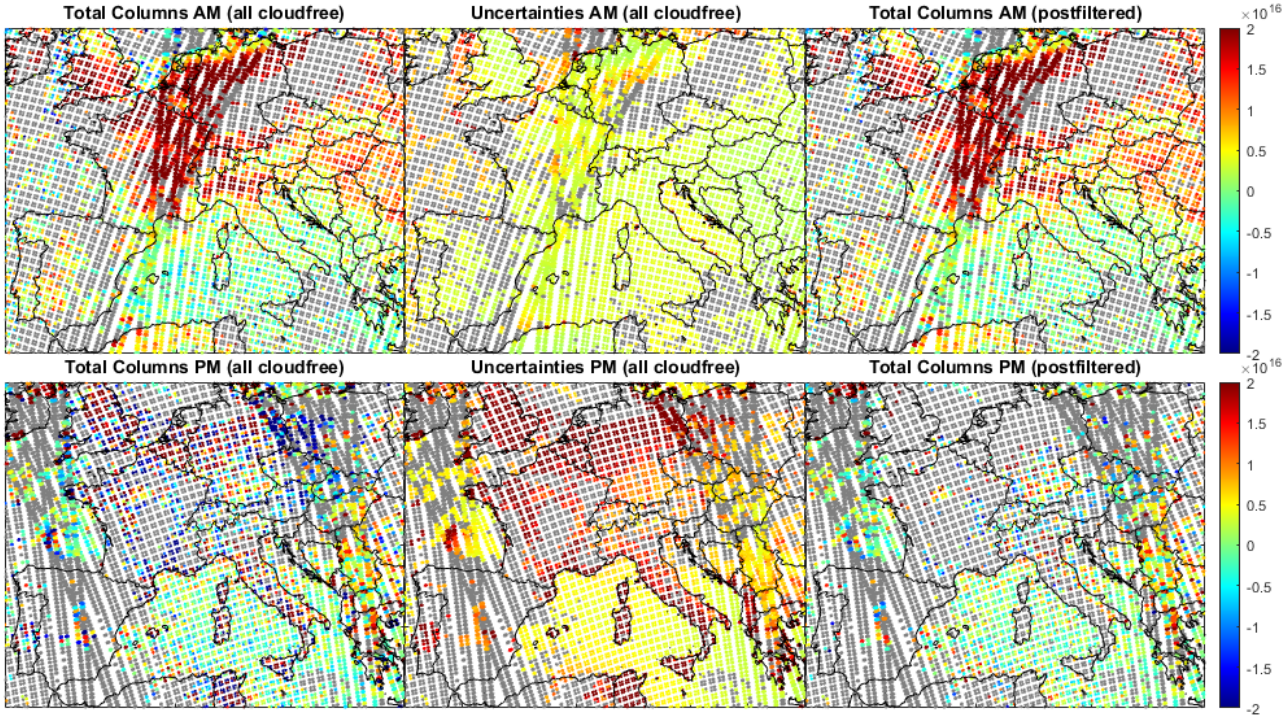

Figure 7. Example NH_3 retrievals from IASI-B on 24 April 2020 (AM, top; PM, bottom). Grey pixels are either cloudy or pixels that do not pass the post filter.

2.3.6 Example: All season average

An all-seasonal average, for 11 year of IASI observations is shown in Figure 8.

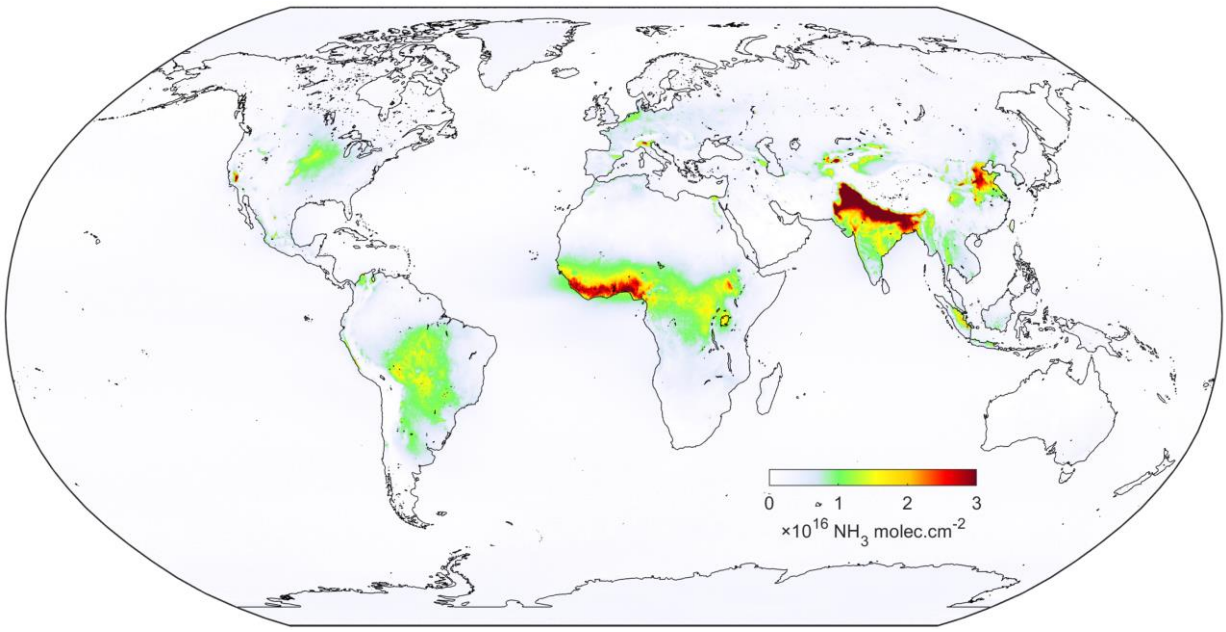

Figure 8 Global average of NH_3 seen by IASI during the morning overpass (2008-2018).

2.4 Advantages of the retrieval algorithm

Computational Efficiency. The only parameter retained from the measurement is the HRI value. Calculating these is straightforward and computational time is negligible. Calculating the neural network function is equally straightforward.

Full Spectral Range. The HRI takes into account a wide spectral range, which contains all the important NH_3 lines in the infrared, and thereby takes full advantage of the thermal infrared.

Low Dependency on the Forward Model. The forward model is only of secondary importance for the calculation of the Jacobians in the HRI and for the HRI calculated from the NN training data.

No A Priori Information. No a priori information on the column is used. This means that all the information from the final measurement comes from the spectral measurement (but potentially with very large associated uncertainties). Therefore, in contrast to optimal estimation approaches, no averaging kernel needs to be applied when carrying out comparison with other measurements/models. A priori information on the vertical profile shape is used though.

Full Atmospheric State. Because the number of input parameters is not limited in the NN, the full temperature, humidity, and pressure profiles can be taken into account. This property is shared with the spectral fitting approaches.

Full Uncertainty Analysis. By perturbing the input parameters, a full uncertainty characterization can be made of how the uncertainty of each of the input parameters propagates to the final result. This analysis can be carried out on a per-pixel basis.

Reduced Bias. Rather than mapping the input parameters directly to a NH_3 column, the output of the NN is a scaling factor, which after multiplication with the HRI gives the column. In this way, the instrumental error on the HRI is translated in a linear way in an error on the column, and negative columns become possible. At the same time, this implies that the algorithm itself is relatively unbiased by design (this is assuming that the HRI values are not biased).

3. REFERENCES

August, T., Klaes, D., Schlüssel, P., Hultberg, T., Crapeau, M., Arriaga, A., O'Carroll, A., Coppens, D., Munro, R., & Calbet, X. (2012) IASI on Metop-A: Operational Level 2 retrievals after five years in orbit. Journal of Quantum Spectroscopy and Radiative Transfer 113, 1340–1371.

Camy-Peyret, C., & Eyre, J. (1998). The IASI Science Plan. Technical report, A Report From The IASI Sounding Science Working Group.

Clarisse, L., Coheur, P. F., Prata, F., Hadji-Lazaro, J., Hurtmans, D., & Clerbaux, C. (2013). A unified approach to infrared aerosol remote sensing and type specification. Atmospheric Chemistry and Physics, 13(4), 2195-2221.

Clarisse, L., Clerbaux, C., Franco, B., Hadji-Lazaro, J., Whitburn, S., Kopp, A., Hurtmans, D., & Coheur, P. F. (2019). A decadal data set of global atmospheric dust retrieved from IASI satellite measurements. Journal of Geophysical Research: Atmospheres, 124(3), 1618-1647.

Clerbaux, C., Boynard, A., Clarisse, L., George, M., Hadji-Lazaro, J., Herbin, H., Hurtmans, D., Pommier, M., Razavi, A., Turquety, S., Wespes, C., & Coheur, P.-F. (2009). Monitoring of atmospheric composition using the thermal infrared IASI/MetOp sounder. Atmospheric Chemistry and Physics, 9, 6041–6054.

Coheur, P. F., Barret, B., Turquety, S., Hurtmans, D., Hadji-Lazaro, J., & Clerbaux, C. (2005). Retrieval and characterization of ozone vertical profiles from a thermal infrared nadir sounder. Journal of Geophysical Research: Atmospheres, 110(D24).

Franco, B., Clarisse, L., Stavrakou, T., Müller, J. F., Van Damme, M., Whitburn, S., Hadji_Lazaro, J., Hurtmans, D., Taraborrelli, D., Clerbaux, C., & Coheur, P. F. (2018). A general framework for global retrievals of trace gases from IASI: Application to methanol, formic acid, and PAN. Journal of Geophysical Research: Atmospheres, 123(24), 13-963.

Hilton, F., August, T., Barnet, C., Bouchard, A., Camy-Peyret, C., Clarisse, L., Clerbaux, C., Coheur, P.-F., Collard, A., Crevoisier, C., Dufour, G., Edwards, D., Faijan, F., Fourrié, N., Gambacorta, A., Gauguin, S., Guidard, V., Hurtmans, D., Illingworth, S., Jacquinet-Husson, N., Kerzenmacher, T., Klaes, D., Lavanant, L., Masiello, G., Matricardi, M., McNally, T., Newman, S., Pavelin, E., Péquignot, E., Phulpin, T., Remedios, J., Schlüssel, P., Serio, C., Strow, L., Taylor, J., Tobin, D., Uspensky, A., & Zhou, D. (2012). Hyperspectral Earth Observation with IASI. Bulletin of the American Meteorological Society, 93(3), 347-370.

Levy, R. C., Remer, L. A., Mattoo, S., Vermote, E. F., & Kaufman, Y. J. (2007). Second-generation operational algorithm: Retrieval of aerosol properties over land from inversion of Moderate Resolution Imaging Spectroradiometer spectral reflectance. Journal of Geophysical Research: Atmospheres, 112(D13).

Van Damme, M., Whitburn, S., Clarisse, L., Clerbaux, C., Hurtmans, D., & Coheur, P. F. (2017). Version 2 of the IASI NH_3 neural network retrieval algorithm: near-real-time and reanalysed datasets. Atmospheric Measurement Techniques, 10(12), 4905-4914.

Van Damme, M., Clarisse, L., Franco, B., Sutton, M. A., Erisman, J. W., Kruit, R. W., van Zanten, M., Whitburn, S., Hadji-Lazaro, J., Hurtmans, D., Clerbaux, C., & Coheur, P. F. (2021). Global, regional and national trends of atmospheric ammonia derived from a decadal (2008–2018) satellite record. Environmental Research Letters, 16(5), 055017.

Walker, J. C., Dudhia, A., & Carboni, E. (2011). An effective method for the detection of trace species demonstrated using the MetOp Infrared Atmospheric Sounding Interferometer. Atmospheric Measurement Techniques, 4(8), 1567-1580.

Whitburn, S., Van Damme, M., Clarisse, L., Bauduin, S., Heald, C. L., Hadji-Lazaro, J., Hurtmans, D., Zondlo, M., Clerbaux, C., & Coheur, P. F. (2016). A flexible and robust neural network IASI-NH_3 retrieval algorithm. Journal of Geophysical Research: Atmospheres, 121(11), 6581-6599.